

Catalytic Pyrolysis of Nonedible Oils for the Production of Renewable Aromatics Using Metal-Modified HZSM-5 Catalysts

Xiaoling Liu, Yafei Wu, Jun Zhang, Yu Zhang, Xun Li, Haian Xia, and Fei Wang*

Cite This: *ACS Omega* 2022, 7, 18953–18968

Read Online

ACCESS |

Metrics & More

Article Recommendations

Supporting Information



ABSTRACT: Catalytic pyrolysis of triglycerides to aromatics over zeolites is an advanced technology for a high value-added utilization of renewable biomass resources. Therefore, in this research, the catalytic performance of M/HZSM-5 catalysts ($M = \text{Zn}, \text{Ga}, \text{In}, \text{Ni}, \text{and Mo}$) during the pyrolysis process of glycerol trioleate and the effect of the compositional difference of several woody oils and waste oils on aromatic formation were investigated. Results revealed that Zn/HZSM-5 with appropriate acidity and metal sites reached the maximum aromatics yield (56.13%) and significantly enhanced the catalytic stability. In addition, these renewable nonedible oils were effectively converted to aromatics over the Zn/HZSM-5 catalyst, the aromatic yield of jatropha oil reached up to 50.33%, and the unsaturation and double bond number of feedstocks were crucial for the production of aromatics. The utilization of biomass resources to produce high value-added aromatics can alleviate the problems caused by the shortage of fossil resources and achieve sustainable green development.

1. INTRODUCTION

Aromatics, especially benzene, toluene, and xylene, are very vital raw materials in the petrochemical industry because they can be widely used in the production of different chemicals, such as polymers, organic solvents, drugs, and dyes.^{1–4} In addition, these aromatics are essential components in the formulation of advanced biofuels within the gasoline range and jet fuel due to an increasing octane number. The traditional aromatics production technologies mainly include the high-temperature dry distillation of coal, hydrogenation of gasoline, aromatization of light hydrocarbons, and catalytic reforming of naphtha,⁵ all of which are heavily dependent on fossil resources and cause environmental pollution by emitting greenhouse gases.⁶ Furthermore, the growing concern about the potential shortage of fossil resources and environmental problems have motivated the interest in developing renewable feedstocks to produce sustainable and bio-based aromatics.⁷

Numerous lignocellulosic biomass feedstocks^{8,9} and model compounds^{10,11} have been used for catalytic pyrolysis to obtain bioaromatics. Nevertheless, the technoeconomic feasibility of aromatics production from solid woody biomass is still under debate due to its complex structure and high oxygen, resulting

in low product yields. In this case, an alternative route for the production of bioaromatics by catalytic pyrolysis of liquid lipid resources is of a great interest. Biomass-derived oils are mainly composed of triglycerides, which have the key advantages of excellent fluidity, high energy density, and a similar molecular structure to fossil resources. Nonedible oil resources, such as jatropha oil, waste cooking oil, and algae, bridge the gap in raw material supply and are preferred as feedstock rather than edible resources to avoid food versus fuel problems.^{12–17} Utilization of these low-cost renewable oils for the production of aromatics not only alleviates the problem of resource shortage but also improves the economic viability of bioaromatics. A brief overview of the catalytic conversion of vegetable oil and model compounds to aromatics was given in Table 1. Aromatics yields vary with the type of vegetable oil

Received: April 1, 2022

Accepted: May 16, 2022

Published: May 27, 2022



and model compounds; this could be due to the differences in the fatty acid composition of oils and reaction conditions.

Table 1. Aromatics Production from Vegetable Oils and Model Compounds

feedstock	catalysts	aromatics yield (%)	ref
oleic acid	Ni-008NaZSM-5	87.46%	41
oleic acid	HZSM-5/Al ₂ O ₃	22 C %	42
canola oil	4%Zn/ZSM-5	42.6%	43
methyl ester			
canola oil	4%Mo/HZSM-5	38.9%	44
methyl ester			
palmitic acid	Y, H β , HZSM-5	43.9 C % (HZSM-5)	45
vegetable oils (3 types)	equilibrium FCC	rapeseed oil: 26%, palm oil: 22%, soybean oil: 24.5%	46
vegetable oils (3 types)	HZSM-5	algal oil: 2.9%, coconut oil: 28% peanut oil: 48%	47
soybean oil	La-Fe/Si-MCM-41	25%	48
rapeseed oil	Ga/ZSM-5, Zn/ZSM-5	Ga/ZSM-5: 43%	49
rubber seed oil	alkali-treated ZSM-5 catalyst	BTX selectivity: 78%	50

Catalytic pyrolysis is considered the most simple and promising approach to producing bioaromatics as a result of feedstock flexibility, a low operational cost, and compatibility with existing petrochemical infrastructure. In fact, the catalyst is the soul of a catalytic conversion, and studies must find ways to ensure better selectivity, a high catalytic activity, and a long service life. Most catalytic cracking and aromatization processes for the production of aromatics have used zeolite catalysts with different pore sizes, such as HZSM-5, Al-MCM-41, beta, USY, and Al-SBA-15.^{18–23} Because the HZSM-5 has an appropriate acid site, a high specific surface area, and an appropriate pore size, it has a better conversion efficiency.^{24–26} However, the most important problem of HZSM-5 as a catalyst is the low yield and the selectivity of the target product, which is related to the relatively narrow pore size and the inappropriate acidity.^{27–32} Many studies have proposed aromatization and coaromatization of lignocellulosic biomass or light hydrocarbons as feed over metal-modified HZSM-5 catalysts to improve the selectivity of HZSM-5 toward aromatics.^{33–36} Aromatization of ethylene has been explored over HZSM-5 modified by the addition of Ag, Mo, Ni, Ga, or Zn due to the presence of metallic species and acid active sites that promote ethylene conversion and aromatization.³⁷ In the study reported by Vichaphund et al.,³⁸ the synthesized metal/HZSM-5 catalysts improved the aromatic selectivity up to 91–97% and decreased the undesirable oxygenates, which loaded metals including Co, Ni, Mo, Ga, and Pd. The dehydrocyclization cracking of soybean oil was tested using Zn-exchanged ZSM-5–Al₂O₃ composite-supported Pt/NiMo sulfide catalysts, where the addition of zinc promoted the formation of aromatics; however, leaching of sulfur may reduce the catalyst activity and cause contamination of products.³⁹ The transformation of jatropha oil into aromatics using a bimetallic ZSM-5 catalyst was investigated in a continuous downflow reactor; the 10Zn5Co5Ce/ZSM-5 catalyst showed an 87.6% oil conversion with 81.9% total aromatics.⁴⁰ These results provide a practical way to prepare catalysts with a high catalytic performance in biomass-derived oil aromatization.

While the performance of the metal-modified catalyst in the conversion of lignocellulosic biomass or light hydrocarbons has been widely reported, few studies have reported the use of nonedible oils as a source of bioaromatics over metal-modified zeolites, and there is no comprehensive comparison of the performance of these catalysts. The reported studies did not consider the variation in product selectivity and yield with the time on stream (TOS) and catalyst stability (lifetime), which are critical to determining the techno-economic potential of vegetable oil synthesis of bioaromatics. In addition, oils obtained from different sources have different fatty acid compositions, which are difficult to compare under different setups and reaction conditions. The use of model compounds such as oleic acid and fatty acid methyl ester have also been widely investigated. In this research, glycerol trioleate was first used as a model compound for the production of aromatic hydrocarbons; one mole of glycerol trioleate is equivalent to three moles of oleic acid, which is more similar in structure to triglycerides from animal fats and vegetables.

Previous studies have found that the impregnation of Ni, Mo, Zn, Ga, and In into zeolite can effectively reduce the content of oxygenated compounds and improve the yield and selectivity of aromatic compounds. Therefore, the HZSM-5 (25) modified with Zn, Ga, In, Ni, and Mo catalysts was prepared by the wet impregnation method, and the physicochemical properties were characterized by different techniques. Glycerol trioleate (GT) was selected as the model compound, Jatropha curcas oil (JCO), rubber seed oil (RSO), tung oil (TO), waste cooking oil (WCO), and waste acidified oil (WAO) were selected as the feedstocks for the production of green aromatics by a catalytic pyrolysis process. In this research, the catalytic activity and catalytic lifetime of different metal-supported catalysts in the conversion of GT were evaluated. In addition, the effect of the composition difference in several woody oils and waste oils representing triglycerides in the formation of aromatics was also comprehensively analyzed.

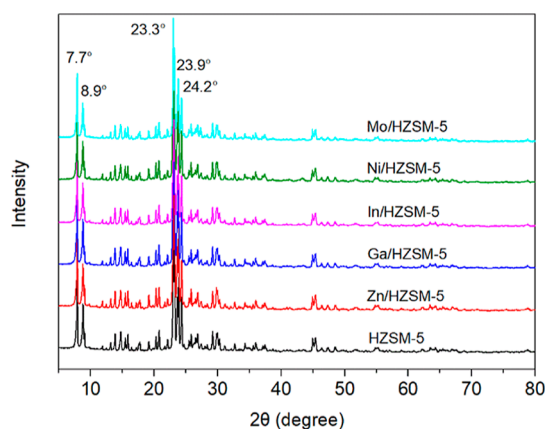
2. RESULTS AND DISCUSSION

2.1. Characterization of Materials. In our previous work, the properties of these five nonedible oils, such as the acid value, saponification value, iodine value, fatty acid, and elemental composition, were studied.⁵¹ As can be seen from Table 2, there were great differences in the composition of these oils. The acid value of waste oil was remarkably higher than that of woody oil, especially the WAO (148.89 mg KOH/g) because it contained a large number of free fatty acids. In addition, these five oils contained a large amount of unsaturated long-chain fatty acids, accounting for 70–94%. Among them, TO contained up to 94% unsaturated fatty acids, mainly eleostearic acid, which is a unique fatty acid with three conjugated double bonds, whereas RSO contained 20% linolenic acid. Elemental analysis showed that these five oils had a high carbon and hydrogen content and a low oxygen content, indicating these feedstocks have an excellent potential in the production of biofuels and chemicals. As shown in the Fourier transform infrared (FT-IR) spectrum of feedstock (Figure S2), the peak at 1745 cm⁻¹ indicated the presence of C=O stretching in –COOR and the C=O stretching vibration of 1710 cm⁻¹ indicated the appearance of carboxylic acid, which confirmed the presence of free fatty acids in these oils.

Table 2. Physicochemical Properties of JCO, RSO, TO, WAO, and WCO

physicochemical properties	JCO	RSO	TO	WAO	WCO
density (g/L)	0.85	0.92	0.91	0.94	0.93
acid value (mg KOH/g)	5.42	22.96	3.78	148.89	99.10
saponification value (mg KOH/g)	183.86	192.70	182.94	188.86	185.99
iodine number (g I ₂ /100 g)	89.42	102.38	141.77	95.02	88.67
fatty acid composition (%)					
palmitic (C ₁₆ :0)	14.29	9.76	2.54	14.42	19.58
stearic (C ₁₈ :0)	6.62	9.85	2.52	4.54	6.91
oleic (C ₁₈ :1)	41.13	24.11	7.41	24.58	34.07
linoleic (C ₁₈ :2)	37.04	35.86	8.35	44.83	30.91
linolenic (C ₁₈ :3)		20.41		5.98	3.48
eleostearic acid (C ₁₈ :3)			78.31		
others	0.92	0.01	0.88	5.65	5.05
total unsaturated fatty acids	78.17	80.38	94.07	75.39	70.65
elemental analysis (%)					
C	76.47	76.59	77.74	76.22	76.41
H	11.77	11.54	10.56	11.94	12.07
N	0.17	0.43	0.63	0.27	0.14
S	0.03	0.01	0.09	0.05	0.02
O	12.10	12.11	12.06	13.09	12.54

2.2. Catalyst Characterization. Crystallinity of different metal-supported catalysts was measured by X-ray diffraction (XRD). The XRD patterns of the parent and metal-modified zeolite catalysts showed the characteristic diffraction peaks of the HZSM-5 zeolite at $2\theta = 7-9^\circ$ and $23-25^\circ$.⁴³ The main peaks of the prepared catalysts were presented at a 2θ of 7.7, 8.9, 23.3, 23.9, and 24.2° (Figure 1). It can be seen that the

**Figure 1.** XRD patterns of the parent HZSM-5 and M/HZSM-5.

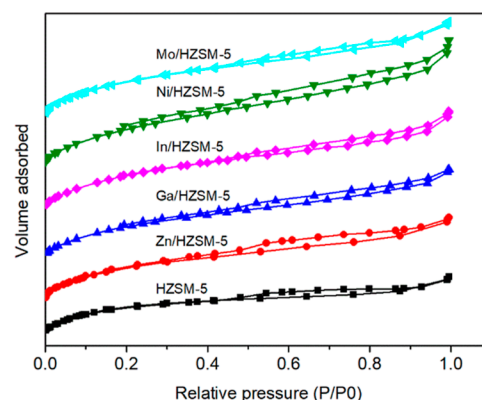
metal-modified catalysts maintain the parent HZSM-5 zeolite structure. In addition, the characteristic diffraction peaks corresponding to metal species were not noticed for any of these M/HZSM-5 catalysts, indicating the metal species that were well-dispersed in the zeolite.

The changes in textural properties caused by the metal introduction during the preparation process were determined by N₂ physisorption. Table 3 lists the textural properties of all

Table 3. Textural Properties and Metal Content of the Parent HZSM-5 and M/HZSM-5

catalysts	surface area (m ² /g)		pore volume (cm ³ /g)		metal loading (wt %)
	S _{BET}	S _{meso}	V _{micro}	V _{meso}	
HZSM-5	387	37	0.15	0.05	
Zn/HZSM-5	410	63	0.15	0.09	1.39
Ga/HZSM-5	398	74	0.14	0.10	0.91
In/HZSM-5	410	96	0.14	0.15	1.39
Ni/HZSM-5	402	71	0.15	0.10	1.65
Mo/HZSM-5	406	69	0.15	0.09	1.03

the catalysts in terms of the total surface area (S_{BET}), mesopore surfaces (S_{meso}), micropore and mesopore volumes (V_{micro} and V_{meso}), and the contents of metal elements. From Figure 2, N₂

**Figure 2.** N₂ adsorption-desorption isotherms of the parent HZSM-5 and M/HZSM-5.

adsorption-desorption isotherms of the metal-modified HZSM-5 were similar to the parent HZSM-5, and all catalysts exhibited a steadily increasing adsorption amount at a low pressure of about 0.05, which corresponded to the transition of nitrogen in the pore of the zeolites from monolayer to multilayer adsorption, which is characteristic of microporous zeolites. However, in the range of $P/P_0 = 0.3-1.0$, all catalysts showed an apparent hysteresis loop, which revealed that the mesopores were introduced into the zeolite micropore structure. For the parent HZSM-5, the value of the total specific surface area, mesopore specific surface area, and size were 387 m²/g, 37 m²/g, and 0.05 cm³/g, respectively. With the impregnation of Zn, the pore volume increased distinctly to 0.24 cm³/g. In/HZSM-5 exhibited a maximal pore volume of 0.29 cm³/g. As expected, the addition of metal species into the HZSM-5 zeolite increased the specific surface area and pore volume of the catalyst to facilitate the mass transfer, which could be attributed to the formation of new pores and surface area during the ion exchange, metal substitution, and calcination process. This phenomenon was also reported by Karnjanakom.⁵² The decrease in the micropore area may be due to metal species blocking the pore channels. However, the textural of M/HZSM-5 catalysts showed that the impregnated metals have a limited influence on the specific surface area and the pore size, probably due to the low content of the loaded metal.

The acid properties of different catalysts were probed by ammonia temperature-programmed desorption (NH₃-TPD) analysis, and the resultant profiles are shown in Figure 3a. To

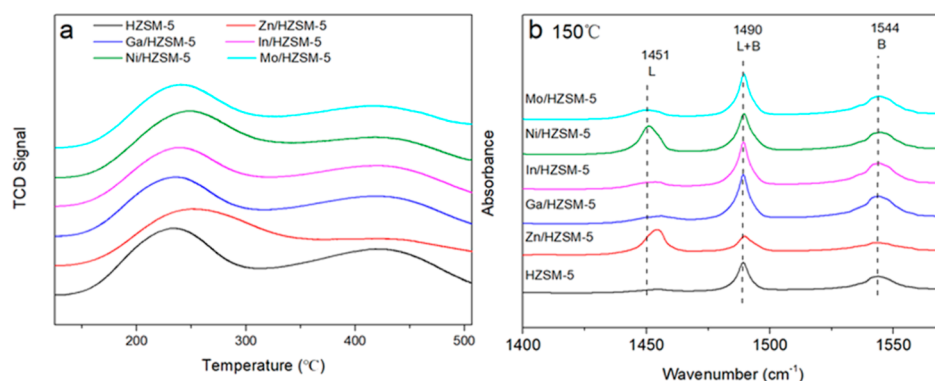


Figure 3. (a) NH_3 -TPD profile and (b) Py-IR spectra of the parent HZSM-5 and M/HZSM-5 catalysts recorded at 150 °C.

further investigate the acidity changes, the specific peak position of the acid, and amount of acid were quantified and presented in Table 4. From Figure 3a, it can be found that, the

Table 4. Distribution of Acid Sites in the Parent HZSM-5 and M/HZSM-5 Catalyst

catalysts	peak temperature, °C		amount of desorbed NH_3 , mmol/g		
	I	II	weak acid	strong acid	total acid
HZSM-5	234	425	0.18	0.20	0.38
Zn/HZSM-5	253	428	0.20	0.12	0.32
Ga/HZSM-5	238	424	0.17	0.18	0.35
In/HZSM-5	241	424	0.17	0.18	0.35
Ni/HZSM-5	248	421	0.22	0.16	0.37
Mo/HZSM-5	241	422	0.19	0.16	0.35

low-temperature peak at about 234 °C and the high temperature peak at around 425 °C can be attributed to NH_3 desorption from weak and strong acid sites, respectively. The NH_3 desorption peaks corresponding to weak acid sites of all catalysts except the Zn-supported ones were shifted gradually toward a higher temperature, while the desorption peaks of strong acid sites were shifted slightly toward lower temperature. It can be seen from Table 4 that the amount of the total acid sites of the M/HZSM-5 catalyst decreased compared with that of the parent HZSM-5, which was mainly due to the decrease in the strong acid amount. Zn/HZSM-5 presented the lowest strong acid amount and total acid amount of 0.12 and 0.32 mmol/g, respectively, but the amount of weak acid increased marginally (0.2 mmol/g). Ni/HZSM-5 displayed the maximum weak acid content (0.22 mmol/g), reduced the content of strong acid (0.16 mmol/g), and moderately decreased the total acid content (0.37 mmol/g). The metal species of Ga and In had a little effect on the strength of acidity and led to a slight loss in the total acidity. The change in the acidity of the catalyst is mainly attributed to the coverage of acidic sites and the interaction of metal species with protonic acids or other groups on the external surface or in the channels; besides, this interaction can convert strong acids to medium or weak acids.^{53,54}

To further distinguish the Brønsted and Lewis acid sites, pyridine-adsorbed infrared spectroscopy (Py-IR) was applied. Figure 3b shows the absorption peaks in the range of 1400–1550 cm^{-1} in the parent HZSM-5 and M/HZSM-5 catalysts; the detailed distribution results of B and L acid sites are listed in Table 5. As shown in Figure 3b, three absorption peaks were detected for all catalysts. The absorption peaks at around 1451

Table 5. Analysis of Acid Properties of the Parent HZSM-5 and M/HZSM-5 Catalysts Recorded at 150 °C

catalysts	total acid ($\mu\text{mol/g}$)	B acid ($\mu\text{mol/g}$)	L acid ($\mu\text{mol/g}$)	B/L
HZSM-5	522.70	473.91	48.79	9.71
Zn/HZSM-5	440.05	217.12	222.92	0.97
Ga/HZSM-5	511.91	445.72	66.18	6.73
In/HZSM-5	474.25	408.74	65.51	6.24
Ni/HZSM-5	551.30	321.94	229.36	1.40
Mo/HZSM-5	464.34	366.95	97.39	3.77

cm^{-1} can be attributed to the absorption of pyridine molecules by L acid sites, and the absorption peaks at 1490 cm^{-1} are simultaneously associated with both B acid sites and L acid sites; moreover, the absorption peaks at 1540 cm^{-1} are assigned to the B acid sites.⁵⁵ Besides, the quantified B acid sites and L acid sites of the parent HZSM-5 were 473.91 and 48.79 $\mu\text{mol/g}$, respectively. As can be observed from Table 5, the incorporation of metals obviously enhanced the L acid sites and regulated the B/L ratio. In the metal-modified HZSM-5, the B acid sites of Zn/HZSM-5 (217.12 $\mu\text{mol/g}$) and Ni/HZSM-5 (321.94 $\mu\text{mol/g}$) were decreased considerably, while the L acid sites were obviously increased (222.92 and 229.36 $\mu\text{mol/g}$, respectively). This may be related to the fact that B acid sites were ion-exchanged with metal species or covered by more Zn and Ni species, resulting in a significant reduction in the concentration of B acid sites. It has been reported that the metal cation could interact with Si–OH–Al in HZSM-5 to form new L acid sites;^{56,57} this may also be responsible for the change in L acid sites. Interestingly, the amount of B acid sites of Zn/HZSM-5 was comparable to the L acid sites with a B/L ratio of 0.97. In addition, the impregnation of Ga and In had a similar effect on the acidity of the catalyst, but the B acid sites of Ga/HZSM-5 were higher than those of In/HZSM-5. The modification of Mo also had a more pronounced effect on acidity compared to Ga and In, and the B/L ratio decreased further. The Py-IR results revealed that the distribution of B and L acid sites were significantly different due to the different interactions between the metal species and HZSM-5 zeolite. On the whole, compared with the parent HZSM-5, the number of B acid sites of M/HZSM-5 was decreased, while the number of L acid sites was increased, and the B/L ratio was reduced.

X-ray photoelectron spectroscopy (XPS) was applied in order to understand the chemical state of different metal species in the HZSM-5 (Figure 4). According to the literature, the active Zn species existing in the form of Zn^{2+} , $[\text{ZnOH}]^+$, and $[\text{Zn–O–Zn}]^{2+58}$ are connected to the zeolite framework.

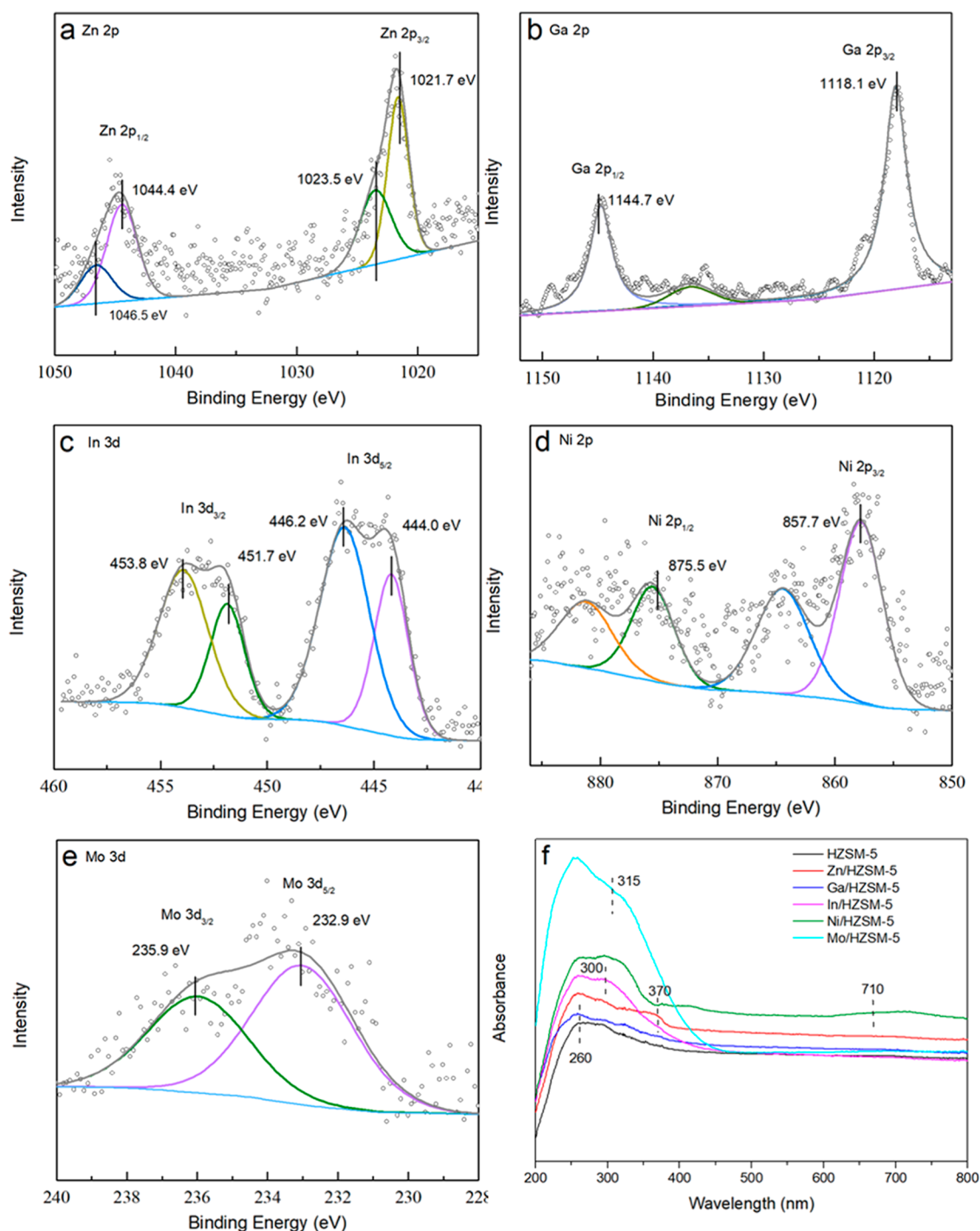


Figure 4. (a–e) XPS spectra and (f) UV–vis spectra of the parent HZSM-5 and M/HZSM-5.

Pure ZnO ($2p_{1/2}$ and $2p_{3/2}$) shows peaks at binding energy of 1021.9 and 1045.0 eV.⁵⁹ The peak appearing at a binding energy of 1022.1 eV for the Zn/HZSM-5 catalyst was ascribed to the ZnO species, and the energy spectrum peak at a high binding energy of 1023.3 eV belonged to the $[\text{ZnOH}]^+$ species.⁶⁰ The increase in the binding energy was probably ascribed to that Zn species and was affected by the oxygen group with a stronger electronegativity than O^{2-} .⁵⁹ It was reported that the intercrystalline size of the Ga species is larger than the pore size of the HZSM-5 zeolites.⁶¹ Thus, Ga species mainly exist in the form of Ga_2O_3 on the external surface of HZSM-5 instead of ion-exchange sites, as observed by the

impregnation method. The XPS spectrum of Ga/HZSM-5 showed only the Ga_2O_3 species at 1118.1 eV.⁶² There were two characteristic peaks of In at 440.7–448 and 448–455.2 eV, both being ascribed to In_2O_3 .⁶³ The fitting peaks of the Ni 2p region were NiO (857.1–860.8 eV for Ni $2p_{3/2}$ and 875.0–878.5 eV for Ni $2p_{1/2}$) and satellite peaks (862.2–864.0 eV for Ni $2p_{3/2}$ and 880.8–882.5 eV for Ni $2p_{1/2}$).⁶⁴ Molybdenum species have many chemical states in zeolite after hydrogen reduction, but only MoO_3 is present by oxidation treatment, and the peaks emerging at 232.9 and 235.9 eV were attributed to MoO_3 .⁶⁵ According to the XPS spectrum of M/HZSM-5, the metal species mainly existed in the form of metal oxides in

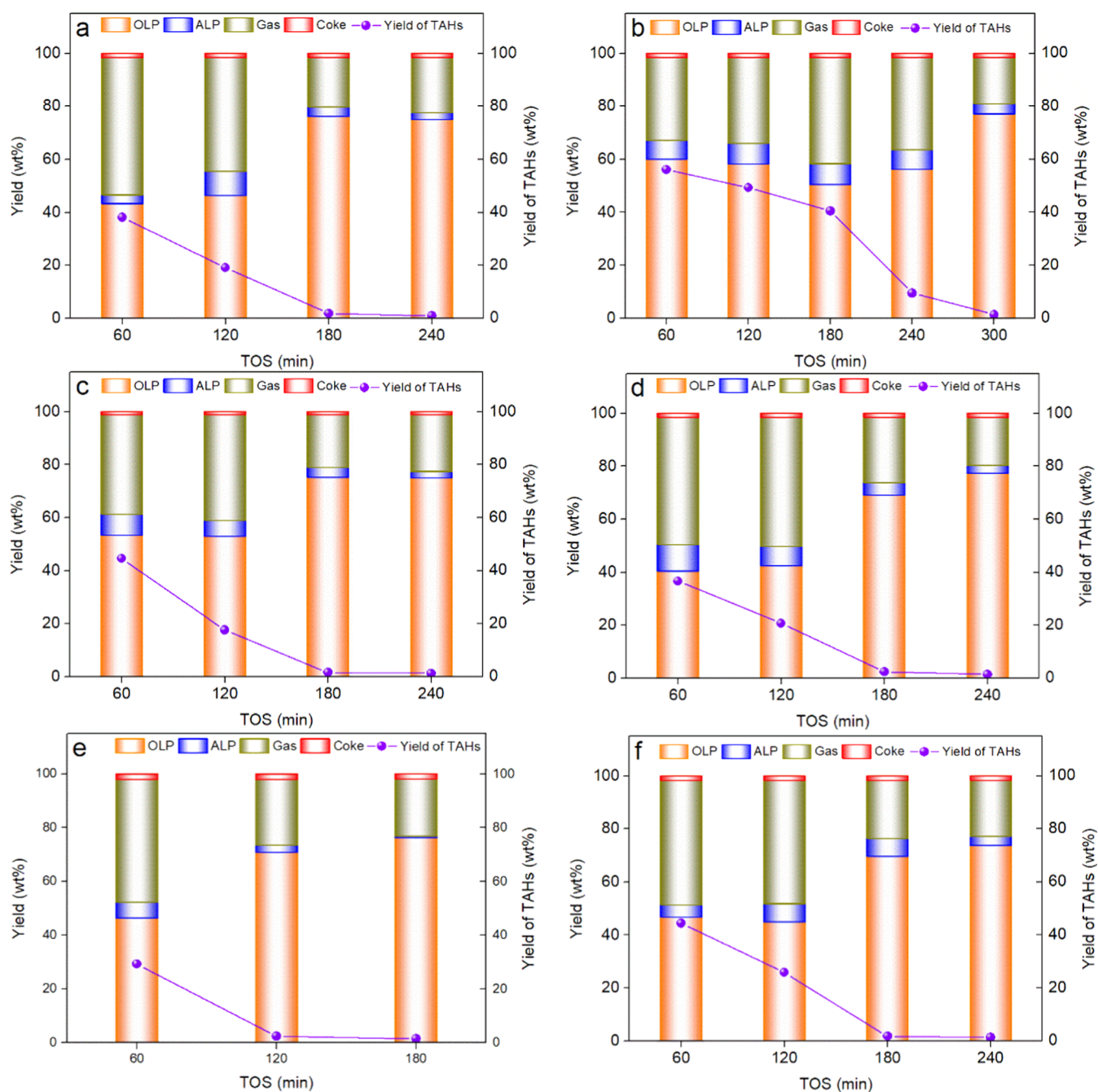


Figure 5. Effect of different catalysts on the product yield with TOS, (a) parent HZSM-5, (b) Zn/HZSM-5, (c) Ga/HZSM-5, (d) In/HZSM-5, (e) Ni/HZSM-5, and (f) Mo/HZSM-5. Reaction conditions: a catalyst loading of 2 g, a catalyst bed temperature of 515 °C, atmospheric pressure, a N₂ flow of 50 mL/min, WHSV of GT of 2.7 h⁻¹.

HZSM-5, and a part of [ZnOH]⁺ also existed in the Zn/HZSM-5 catalyst.

The coordination states of the prepared catalysts were investigated by the UV–visible diffuse reflectance spectrum (Figure 4). All prepared catalysts exhibited a large broad absorption peak at 200–400 nm. However, the characteristic peaks of each catalyst also appeared. The peak at 370 nm corresponded to ZnO crystallites.⁶⁶ The absorption peak at 260 nm was the characteristic peak of the Ga₂O₃ valence band to conduction band electronic transition, which indicated that in the Ga/HZSM-5 catalyst, gallium existed in the form of Ga₂O₃.⁶⁷ The spectrum of In/HZSM-5 was represented by an absorption peak in the UV region with an extended absorption

edge at about 200–260 and around 300 nm. These peaks can be associated with the bulky In₂O₃ species located on the external surface of the zeolite crystallites.⁶⁸ The spectra of the nickel-containing catalyst show a wide peak around 710 nm, which may be due to the contribution of the nickel oxide species.⁶⁹ In the spectrum of Mo/HZSM-5, a peak at 315 nm was detected and assigned to the crystalline MoO₃ phase.⁷⁰ Both the UV–visible diffuse reflectance spectrum (DRS) and XPS results confirmed that the metal species mainly existed in the zeolite in the form of metal oxides.

2.3. Catalytic Pyrolysis of Nonedible Oil. The catalytic performance of different metal-supported catalysts for GT was investigated in a fixed-bed reactor. In addition, the effect of the

composition difference of several renewable woody oils and waste oils on the formation of aromatics was also comprehensively analyzed.

2.3.1. Effect of Different Catalysts on the Product Yield in the Catalytic Pyrolysis of Glycerol Trioleate. The effect of the catalyst on the product yield and the yield of total aromatic hydrocarbons (TAHs) was evaluated (Figure 5). The composition of the organic liquid products versus TOS was determined by FT-IR (Figure S3) and GC-MS analysis (Figures S4 and S5). At the TOS of 240, 300 min, the peaks at 1745 and 1710 cm^{-1} appeared in the FT-IR spectrum, indicating that the formation of aromatics became negligible and abundant oxygenated macromolecules were generated. GT and other oxygenated hydrocarbons were typically not present in the liquid phase at an early stage of reaction, indicating the strong catalytic cracking ability of the catalysts and a complete conversion of the feedstock.

The liquid hydrocarbons, noncondensable gas, and coke obtained by the catalytic pyrolysis of GT with different metal-loaded catalysts are shown in Figure 5. The metal-modified catalysts (except In), especially the Zn modification, significantly enhanced the generation of liquid hydrocarbon products at the expense of gaseous products compared to the parent HZSM-5. At a TOS of 60 min, higher liquid yields were achieved for the Zn/HZSM-5 and Ga/HZSM-5 catalysts of 60.17 and 53.40%, respectively. In/HZSM-5 produced the lowest liquid yields compared with the parent HZSM-5, which decreased by 40.47%. This is because of the remarkable dehydrogenation and deoxygenation of Ga and Zn, which facilitate the pyrolysis reaction of oils and direct degradation of large molecular substances into smaller molecules. Meanwhile, the metal-loaded catalyst (except Ni) could effectively decrease the coke deposit. This may be due to the fact that the metal loading introduced more mesopores to facilitate the diffusion of primary products. The B acid sites are the main active site for cleavage, deoxygenation, and aromatization reactions. When the catalyst was modified, the B acid sites and the strong acid content were decreased, thus preventing excessive aromatization and inhibiting coke deposition.

It is worth noting when the GT underwent catalytic pyrolysis by Zn/HZSM-5 (Figure 5b) at a TOS of 60 min, the yield of OLPs reached 60.17%, and the yield of aromatics achieved a maximum of 56.13%, which were 16.91 and 18.01% higher than those of the parent HZSM-5 catalyst (43.26 and 38.12%, respectively). The aromatization process is considered to be a series of extremely complicated steps, including the steps of alkanes activation, oligomerization, cyclization, and dehydrogenation. The acidity of the catalyst plays an essential role in this process, with the B acid sites promoting the formation of cycloalkanes and the formed cycloalkanes being transferred to the L acid sites for deoxygenation and aromatization steps to generate aromatics. It has been demonstrated that the yield of aromatics is directly proportional to the number of L acid sites, and there is a linear relationship between the amount of the $[\text{ZnOH}]^+$ species and the selectivity of aromatics over Zn/HZSM-5 catalysts.^{37,71} According to Py-IR results, Zn/HZSM-5 exhibited sufficient acid sites, L and B acidic sites were in balance, and the B/L ratio was 0.97. Based on the XPS results, it is clear that the Zn species in Zn/HZSM-5 were presented in the form of ZnO and $[\text{ZnOH}]^+$ (as L acid sites), which not only facilitated the acidity regulation but also promoted the dehydrogenation reaction as a metal active site. These may be two reasons for

the Zn/HZSM-5 catalyst enhanced production of liquid products and aromatics. In addition, Ga species as a dehydrogenation active center has a synergistic effect with the acid center of HZSM-5, so the addition of Ga can promote the dehydrogenation and cyclization reactions of olefins, thus increasing the aromatics yield to 44.62%. It was reported that the isolated Ga_2O_3 on the outer surface of the HZSM-5 zeolite has a limited exchange of proton acid with zeolite, and the hydrogen pretreatment leads to the formation of new catalytic centers (Ga-Lewis), which favor the formation of aromatics.⁷² The introduction of Ga reduced the content of B acid while increasing the L acid content distinctly; however, the difference in the content of L acid and B acid was so considerable that reactions occurring at the L acid site would be inhibited. Thus, Ga/HZSM-5 without hydrogen reduction could not have enough catalytically active centers and contributed less to the aromatic formation than the Zn-containing catalyst.

Compared with that of the parent HZSM-5, the aromatization ability of Mo/HZSM-5 (Figure 5f) was slightly improved (44.40%) and that of In/HZSM-5 (Figure 5d) has no obvious promotion effect. This may be explained by a lower cracking activity of Mo and In-containing catalysts compared to the other metal-containing catalysts. In addition, from the characterization results of the catalysts, the pore structure, and L acid properties of HZSM-5 modified with Ga and In were similar, but the cracking and aromatization ability of Ga was stronger than that of In, which indicated that the catalytic performance was related to the synergistic effect of the metal type, B acid sites, and L acid sites. This finding could be attributed to the introduction of In by impregnation in the form of indium oxide dispersed on the external surface of HZSM-5; these indium oxide species were unable to act as metal active sites and thus reduced the role of cracking and aromatization reactions.

A different phenomenon is that for the catalytic pyrolysis of GT over Ni/HZSM-5 (Figure 5e), where the aromatization ability dropped sharply after 60 min of the reaction, and the yield of aromatics was almost negligible after 180 min. Moreover, Ni/HZSM-5 had a higher coke yield (2 wt %) compared to the parent HZSM-5. After the excessive Ni-modified HZSM-5, the Lewis acid also became excessive, which promoted the continuation of the dehydrogenation reaction to form aromatics; however, the excess dehydrogenation resulted in a large amount of polycyclic aromatic hydrocarbons (PAHs) and coke deposits blocking the zeolite pores, and reducing the yield of aromatics. To sum up, in the catalytic pyrolysis of GT over M/HZSM-5 catalysts, a higher yield of the organic liquid products formation was found in the following order: Zn/HZSM-5 > Ga/HZSM-5 > Mo/HZSM-5 > Ni/HZSM-5 > HZSM-5 > In/HZSM-5, and the order of the aromatization effect of different loading metals was as follows: Zn/HZSM-5 > Ga/HZSM-5 > Mo/HZSM-5 > HZSM-5 > In/HZSM-5 > Ni/HZSM-5.

At prolonged TOS, the yield of OLPs increased from the initial 45 to 75%, while the yield of TAHs gradually reduced from 57 to 2%, which was due to the weakening of the catalytic ability. According to GC-MS results (Figure S4), saturated and unsaturated hydrocarbons with a carbon chain length of 6–16 and oxygen-containing macromolecules were found in the products at a later stage of reaction, which was also the reason why the yield of the organic liquid products increased with the increasing TOS. When the decarboxylation and dehydration reaction degrees were reduced, the oxygen-

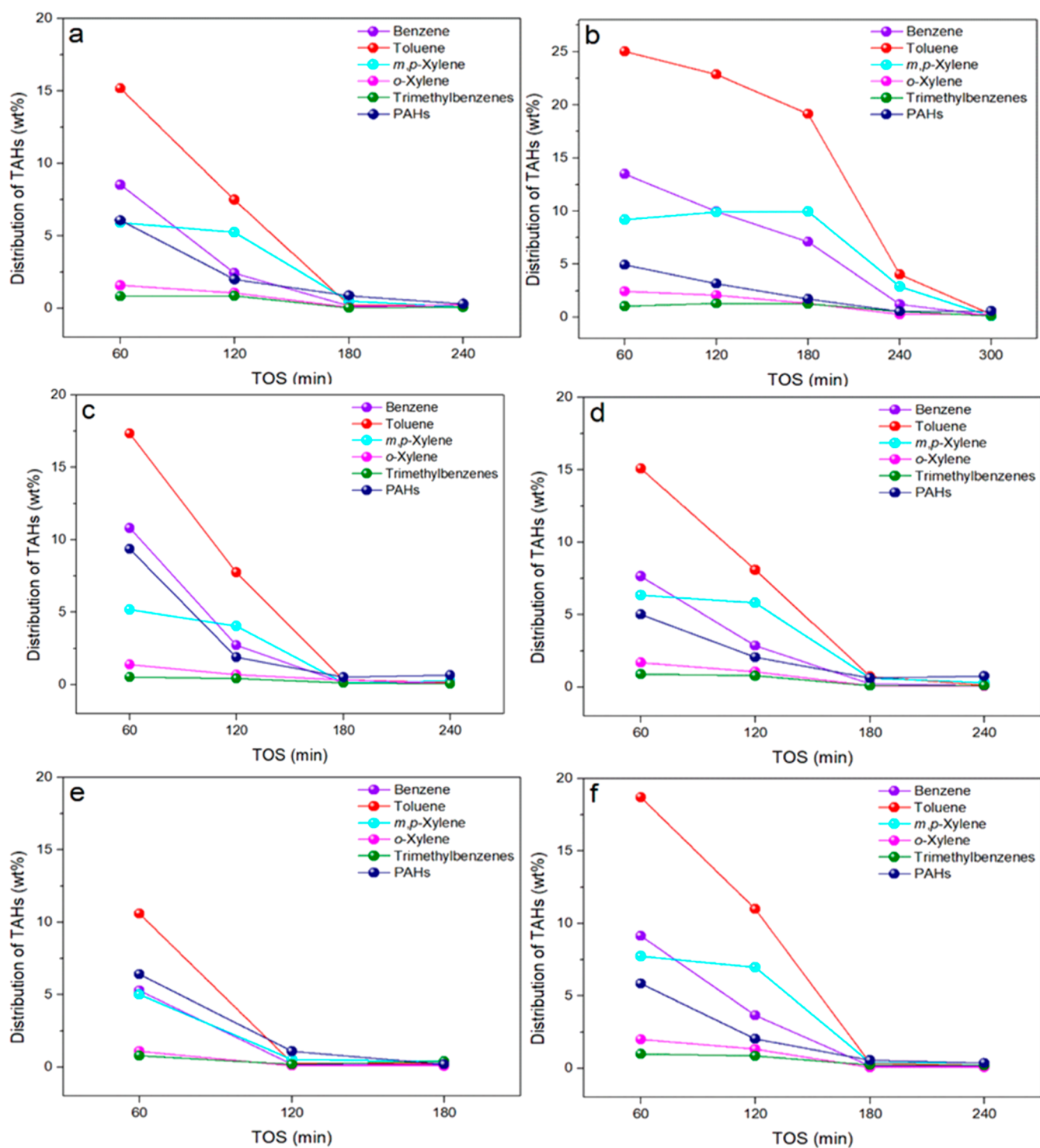


Figure 6. Effect of different catalysts on the fraction of aromatic products with TOS, (a) parent HZSM-5, (b) Zn/HZSM-5, (c) Ga/HZSM-5, (d) In/HZSM-5, (e) Ni/HZSM-5, and (f) Mo/HZSM-5. Reaction conditions: a catalyst loading of 2 g, a catalyst bed temperature of 515 °C, atmospheric pressure, a N₂ flow of 50 mL/min, and WHSV of GT of 2.7 h⁻¹.

containing compounds increased. At the same time, excessive oxygen-containing macromolecules covered the external surface of the catalyst and hindered the accessibility to the active sites. As a result, the catalytic efficiency was reduced, and the aromatic content was decreased. The Zn/HZSM-5 catalyst was deactivated after a TOS of 300 min, the Ni/HZSM-5 catalyst was deactivated after a TOS of 180 min, and the other catalysts were deactivated after a TOS of 240 min. This indicates that

the Zn species significantly prolonged the catalytic lifetime and enhanced the catalytic stability probably due to the introduction of an appropriate amount of mesopores and modulation of the catalyst acidity.

2.3.2. Effect of Different Catalysts on the Aromatic Selectivity in the Catalytic Pyrolysis of Glycerol Trioleate. The main components of aromatic hydrocarbons obtained by the catalytic pyrolysis of GT over the parent HZSM-5 and M/

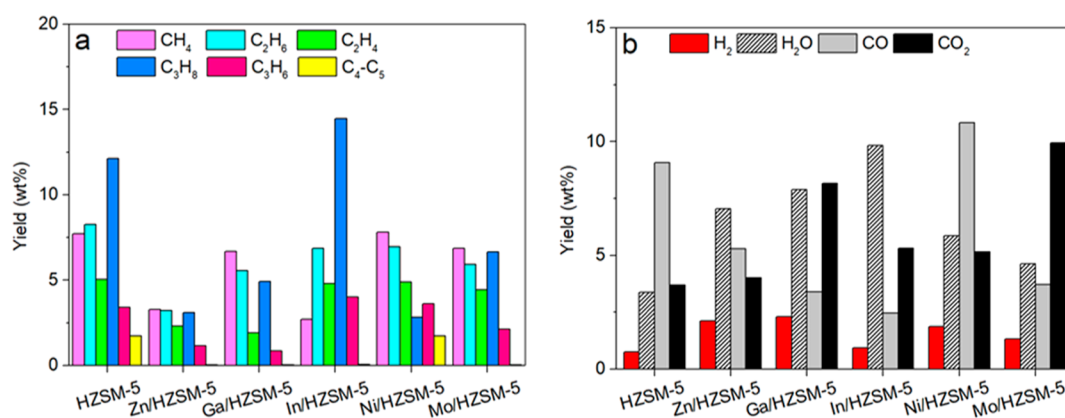


Figure 7. Effect of the different catalysts on the distribution of the gaseous product, (a) yield of C_1 – C_5 light hydrocarbon gas products, (b) yield of H_2 , H_2O , CO , and CO_2 . Reaction conditions: a catalyst loading of 2 g, a catalyst bed temperature of 515 °C, atmospheric pressure, a N_2 flow of 50 mL/min, WHSV of GT of 2.7 h^{-1} .

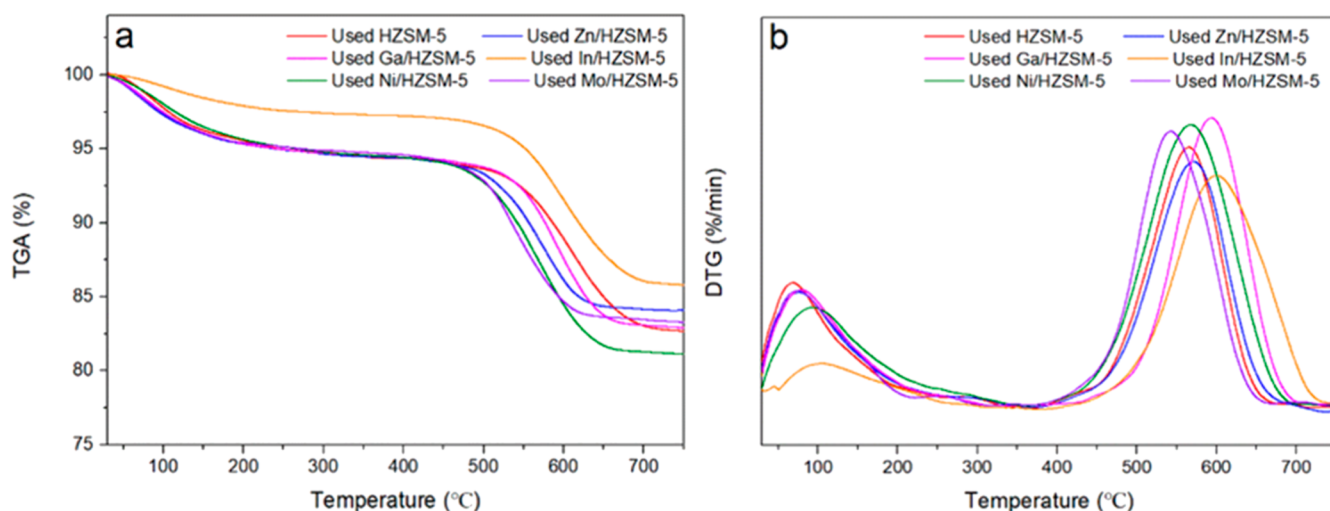


Figure 8. Thermogravimetric analysis of the used catalysts, (a) weight loss as a function of temperature, and (b) derivative weight loss as a function of temperature.

HZSM-5 were detected by GC (Figure 6). In the catalytic pyrolysis process, a wide range of hydrocarbons such as alkanes, alkenes, monocyclic aromatic hydrocarbons (MAHs), and PAHs were found in the OLPs. It was more encouraging that a large number of hydrocarbons were concentrated in the range of aromatic hydrocarbons (~96%), especially C_6 – C_9 MAHs. These were benzene, toluene, ethylbenzene, xylene, trimethylbenzene, naphthalene, 1-methylnaphthalene, 2-methylnaphthalene, and other aromatics. At the TOS of 60 and 120 min, these M/HZSM-5 catalysts generated mainly toluene with a yield of 15–25%, while the yield of benzene was 8–13%, and the yield of xylene was 7–14%. With a longer TOS, the selectivity of the catalyst to aromatics decreased gradually. At a TOS of 60 min, Zn species mainly promoted the formation of benzene (13.50%), toluene (25.04%), and xylene (11.64%), Ga mainly increased the yield of benzene (10.82%) and toluene (17.34%), In had no obvious promotion effect, Ni inhibited the formation of BTX, while Mo had a little influence on the information of MAHs except toluene. On the other hand, Zn, In, and Mo species inhibited the formation of PAHs. These findings were related to the pore size and acidity of the catalyst. The Ga and Zn species were highly dispersed in HZSM-5, which allowed the pyrolysis intermediates to come into full contact with the metal active sites and the acidic sites of

HZSM-5, and further reactions resulted in a pronounced improvement in the selectivity of the aromatics. When Ga was loaded, the strong acid and the B acid sites content were higher compared to other metal species, which promoted the polymerization of light aromatics to form PAHs. When the Ni/HZSM-5 catalyst was used, the pore size of the catalyst was decreased owing to enrichment of more nickel species, hindering the transfer of light aromatics. The Ni/HZSM-5 catalyst had the highest total acid and L acid site content, enhancing the cyclization and polymerization of intermediates to form PAHs. PAHs such as biphenyl, anthracene, and phenanthrene are one of the causes of coke formation and lead to catalyst deactivation, so the generation of PAHs should be avoided. From the above results, benzene, toluene, and xylene (BTX) are the main aromatics, and different metal species have different selectivity for aromatics due to the synergistic effect of acidity and metal active sites, and Zn, In, and Mo species possess the ability to inhibit the formation of PAHs.

2.3.3. Effect of Different Catalysts on the Gas Products in the Catalytic Pyrolysis of Glycerol Trioleate. Within a TOS of 60 min, the gas product distribution of catalytic pyrolysis of GT over the prepared catalyst was also evaluated. All gas products contained CO , CO_2 , H_2 , and light hydrocarbons (CH_4 , C_2H_6 , C_2H_4 , C_3H_8 , and C_3H_6 , C_4 – C_5). According to

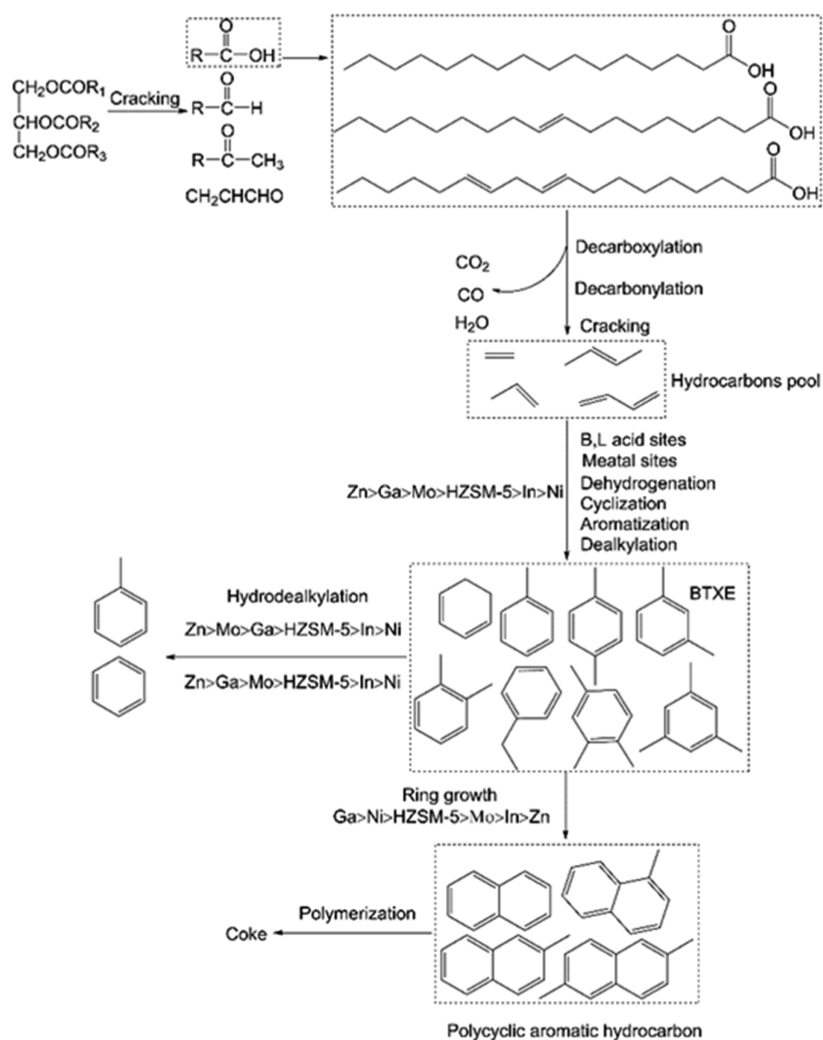


Figure 9. Reaction pathways for the aromatics production from GT over metal-modified HZSM-5 catalysts.

Figure 7a, the addition of metal into the HZSM-5 zeolite had various degrees of change in the distribution of light hydrocarbons, which were mainly reflected in a decrease in the ethylene and propylene yields. It was worth noting that this effect was quite more pronounced for the Zn and Ga modification, and the olefins yields were about half of those obtained over the parent HZSM-5. However, the reduction in olefins was not accompanied by an increase in ethane and propane production, indicating that it was not caused by the hydrogenation pathway of olefins. The decrease in light olefin production may be due to the cracking reaction or the consumption of ethylene and propylene through the oligomerization, cyclization, and aromatization reaction. Compared to other metal loadings, the formation of C_1 – C_4 alkanes and C_2 – C_4 alkenes were favored over the Ni-impregnated catalyst. The oxygen present in the GT can be removed by decarbonylation, decarboxylation, and dehydration, which lead to the formation of CO , CO_2 , and H_2O (ALP), respectively.⁷³ Starting with the parent HZSM-5, the B acid sites rather enhanced the decarbonylation more than the decarboxylation reaction,⁶⁶ resulting in a high amount of CO and a lower amount of CO_2 . Compared with the parent HZSM-5, the CO_2 and H_2O yield increased obviously over M/HZSM-5 catalysts, indicating that the addition of metals and the change in acidity for the HZSM-5 catalyst were beneficial

for the deoxygenation. Other multiple chemical reactions such as deoxidation and dehydrogenation caused the production of hydrogen and light hydrocarbons.¹³ The above results indicated that the loading of metal to HZSM-5 facilitated the reactions including decarbonylation, decarboxylation, dehydrogenation, and aromatization during the catalytic pyrolysis process.

2.3.4. Effect of Different Catalysts on Coke in the Catalytic Pyrolysis of Glycerol Trioleate. It is well-known that coke deposition is the main cause of catalyst deactivation. Coke in zeolite is formed mainly from heavy hydrocarbons, which may be located on the externals and also inside the channels of zeolite.⁷⁴ As can be seen from the Figure 8a, the weight loss was mainly at 100–200 and 400–600 °C. The former was due to evaporation of the adsorbed water in the catalyst, whereas the latter could be related to the combustion of coke deposited on the active metal and support. In the case of the parent HZSM-5, the total amount of coke was 12.23%, referred to as the tested catalyst. The metal-modified HZSM-5 catalysts (except for the nickel loading) were all shown to reduce the coke content. Zinc loading slightly reduced the coke amount, while nickel loading increased the coke amount by 2%. This result was in agreement with a previous work,²⁹ which indicated that the presence of nickel promote the formation of coke over the zeolite catalyst, which was

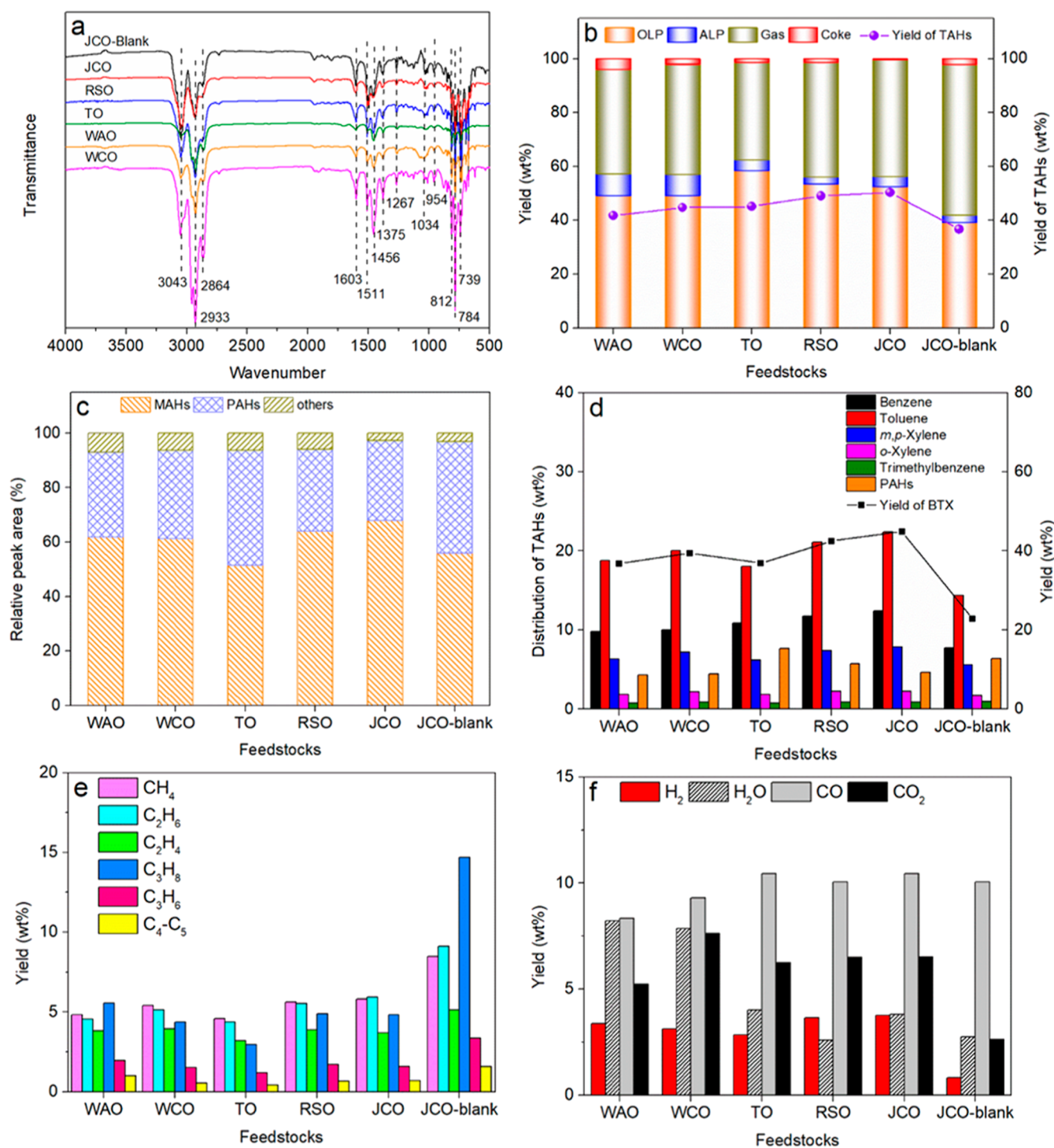


Figure 10. Effect of the different feedstock on the product yield and the properties of OLPs over the Zn/HZSM-5 catalyst: (a) FT-IR spectra of OLPs, (b) yield of products and TAHs, (c) composition of OLPs based on GC-MS, (d) aromatic hydrocarbon distribution of OLPs based on GC, (e) distribution of the light hydrocarbon gas product, and (f) fraction distribution of gas products. Reaction conditions: the Zn/HZSM-5 catalyst of 2 g, a catalyst bed temperature of 515 °C, atmospheric pressure, a N₂ flow of 50 mL/min, and WHSV of feedstocks of 2.7 h⁻¹.

responsible for the rapid deactivation of the impregnated nickel catalyst. Figure 8b shows the weight loss peaks for each type of catalyst at different temperatures, indicating that there were important variations in terms of the nature and location of coke.⁷⁵ From a smaller DTG peak of Zn/HZSM-5, it is evident that the zinc metal species could mitigate the formation of coke. A very large DTG peak was presented in Ni/HZSM-5, and the peak position shifted to a higher temperature,

indicating the formation of a more difficult to remove coke, possibly from the polymerization of more PAHs. For the Ga- and In-containing catalysts, the peaks were at 600 °C, indicating the formation of hard coke that needs a higher temperature to be removed or that these cokes were located on metal sites.⁷⁶

In short, the characterization results of the modified catalysts showed that the incorporation of metals had a limited

influence on the structure but caused a significant change in acid properties. However, the change in acid properties and metal species played a vital role in the aromatization ability and stability of the catalyst. A simplified summary of the reaction pathways for the observed relativities is presented in Figure 9.^{33,40,77,78}

2.3.5. Catalytic Pyrolysis of Woody Oils and Waste Oils. Five different nonedible oils (JCO, RSO, TO, WCO, and WAO) were selected as triglyceride feedstocks to produce aromatics through the catalytic cracking and aromatization of the Zn/HZSM-5 catalyst, and the effect of feedstock composition on the product yield and properties of the organic liquid product were investigated.

In the FT-IR spectra of OLPs obtained by Zn/HZSM-5 (Figure 10a), a vanishing band was observed at 1745 and 1710 cm^{-1} , which confirmed the complete conversion of feedstocks and a higher degree of deoxygenation. The peaks at 1603, 1034, 784, and 739 cm^{-1} confirmed the abundant aromatic hydrocarbons in the OLPs.

Figure 10b showed that the catalytic pyrolysis of all these five oils resulted in high yields. The yield of OLPs obtained by TO was the highest (58.43%), the aromatics yield accounted for 45.17%, the yield of OLPs obtained by WAO was the lowest (49.14%), the aromatics yield accounted for 41.76%, the yield of OLPs and aromatics obtained by WCO reached 49.20 and 44.73%, respectively, the yield of OLPs obtained by JCO accounted for 52.57%, the aromatics yield was the highest (50.33%), and the yield of aromatics obtained by RSO was lower than JCO. The order of decrease in the liquid product yield was TO > RSO > JCO > WCO > WAO, and the order of decrease in the TAHs yield was JCO > RSO > TO > WCO > WAO. As can be observed from Figure 10b, the liquid products and aromatics obtained from woody oil were higher than those from waste oil, which may be due to the high percentage of free fatty acids in waste oil. It is difficult to compare these yields with the literature data as large differences in reaction conditions and reactor types are applied. However, the overall yields of aromatics in this study were in the range within or even higher than those reported for canola oil, coconut oil, palm oil residue, and wasted cooking oil (30–40%).⁴² Compared to other oils, the catalytic pyrolysis of TO produced fewer aromatics, which may be attributed to its peculiar fatty acid with three conjugated double bonds. It is also found that the Zn-modified catalysts can enhance the liquid product and aromatics formation compared with the parent HZSM-5 catalyst (39.28–58.43 and 36.68–50.33%, respectively). It can be concluded that the Zn/HZSM-5 catalyst has a wide range of applications for triglyceride feedstocks and that these nonedible oils can be used to produce aromatics.

The composition and distribution of OLPs was based on GC–MS analysis, and the liquid products were mainly C_6 – C_{12} hydrocarbons, including about 95% aromatics and a small fraction of alkanes and alkenes, of which monocyclic aromatics accounted for 50–70%. Compared to other oils, the TO catalytic conversion produced more PAHs, including naphthalene, methylnaphthalene, and others, which may be due to the polymerization of unsaturated macromolecules. The percentage distribution of aromatics based on GC is shown in Figure 10d, where BTX were the main components, with toluene accounting for 18–22%, benzene for 9–13%, and xylene for 7–10%. The Zn species greatly enhanced the formation of monocyclic aromatics. In the catalytic cracking

and aromatization reaction of JCO over Zn/HZSM-5, the maximum yield of BTX was 44.86%.

The gas product distribution of five oils' catalytic conversion are shown in Figure 10e,f. Compared with the parent HZSM-5, the gas yield of Zn-supported catalyst catalytic pyrolysis was reduced, and the yield of light hydrocarbons was not much different, but the yield of hydrogen and carbon dioxide increased observably, indicating that the zinc modification enhanced the dehydrogenation and deoxygenation capabilities. The existence of H_2 was beneficial for the hydrocracking of the pyrolysis intermediates and stabilizing the pyrolytic fraction, which could prevent polymerization from coking. In the catalytic pyrolysis of JCO on the parent HZSM-5 catalyst, methane, ethane, and propane were the main light hydrocarbon components, of which propane accounted for the largest percentage (14.7%). The gas product distributions obtained from JCO and RSO were similar over the Zn/HZSM-5 catalyst, and the ethylene content was lower than that of light alkanes.

In summary, in the presence of the Zn/HZSM-5 catalyst, these nonedible oils were well-converted into aromatics. When using JCO as the raw material, the aromatic yield reached 50.33%. The degree of unsaturation and the number of double bonds of feedstock were of significant importance to regulate the product distribution and aromatics selectivity. These results are potentially attractive for the implementation of processes for the commercial production of aromatics from feedstocks of different origins, which can alleviate the problems caused by fossil resource shortages, reduce our dependence on fossil resources, and achieve sustainable development of green biomass resources.

3. CONCLUSIONS

In this study, the catalytic cracking and aromatization performance of the metal-modified HZSM-5 catalyst in the pyrolysis of GT to generate aromatics and the effect of the nonedible oil composition on the products were investigated. The results revealed that metal species and acidity have a vital effect on the formation of aromatics, and Zn/HZSM-5 with an appropriate acidity and metal sites was favorable for catalytic cracking and aromatization of triglycerides to produce aromatics. In addition, nonedible oils were well-converted into aromatics by Zn-supported catalysts, and the degree of unsaturation and the number of double bonds of feedstock were of vital importance to the synthesis of aromatics.

At present, the production of bioaromatics by the catalytic pyrolysis of oils is not available on a commercial scale, which is related to the availability of feedstocks and suitable catalytic systems and catalytic reactors. The addition of metal species into zeolites is proposed to modify the acid and textural properties of the support improving its catalytic performance. Future research work will also continue to focus on the development of highly selective catalysts. The catalyst design should be improved by suitable modifications and optimization with the ultimate goal of the new catalyst to produce a higher selectivity for value-added biofuels or aromatics.

4. EXPERIMENTAL SECTION

4.1. Materials. GT was selected as the triglyceride model compound. JCO, RSO, TO, WCO and WAO were selected as the triglyceride feedstocks for the production of aromatics by the catalytic pyrolysis process. GT (Sinopharm Chemical

Reagent Co., Ltd, CP,60%) and TO were obtained commercially, JCO and RSO were extracted from their seeds using a pressing method, and WCO and WAO were obtained from restaurants and industrial source.

4.2. Catalyst Preparation. The untreated HZSM-5 zeolite with a Si/Al ratio of 25 was obtained from the Catalyst Plant of Nankai University. In order to remove impurities from the untreated HZSM-5 zeolite, an ion exchange was performed with a NH_4Cl solution to convert the H-type to NH_4 -type, and NH_4^+ were removed and converted to the H-type by calcination. 100 mL of a 1 M NH_4Cl solution was added into the untreated HZSM-5 zeolite (the ratio of zeolite mass to volume of the NH_4Cl solution was 1/20). The mixture of the HZSM-5 zeolite and NH_4Cl solution was stirred at 25 °C for 2 h. After that, the zeolite was separated by filtration and washed three times with deionized water in order to remove residual chloride ions. The washed sample was dried at 120 °C for 8 h and then calcined in oxygen atmosphere at a heating rate of 2 °C/min from room temperature to 550 °C for 2 h to obtain the parent HZSM-5 catalyst.

The M/HZSM-5 (M = Zn, Ga, In, Ni, or Mo) catalysts were prepared by wet impregnation methods. The theoretical mass fraction of the load metal is 1.3%. In a typical impregnation process, a certain concentration of an aqueous solution of Zn (NO_3)₂, Ga (NO_3)₃, In (NO_3)₃, Ni (NO_3)₂, and (NH_4)₆Mo₇O₂₄ was added into the parent HZSM-5 catalyst of 5 g (the ratio of parent HZSM-5 mass to volume of the metal salt solution was 1/20) under stirring at 25 °C for 2 h, then the mixture was continuously stirred and heated to dryness at 85 °C. M/HZSM-5 catalysts were obtained by drying at 120 °C for 8 h and calcining in oxygen atmosphere at a heating rate of 2 °C/min from room temperature to 550 °C for 2 h.

4.3. Catalyst Characterization. The prepared catalysts were characterized by powder XRD, N_2 physical adsorption–desorption, XPS, UV–visible DRS (UV–vis DRS), NH_3 –TPD, and Py-IR. The metal element contents of the prepared catalysts were measured by inductively coupled plasma optical emission spectrometry (ICP-OES). The amount of coke deposited over the catalyst after the reaction experiments was measured by thermogravimetric analysis (TGA). The detailed instrument information and analysis methods are listed in the [Supporting Information](#).

4.4. Catalytic Pyrolysis of Nonedible Oils. The catalytic pyrolysis of nonedible oils was carried out in a laboratory-scale fixed-bed reactor. The fixed-bed reactor tube was made of quartz with an inner diameter of 2 cm and a length of 60 cm. The experimental setup included a water bath pot, a feedstock tank and pump system, a nitrogen and oxygen cylinder with a gas mass flow meter, a tubular fixed-bed reactor, and an electric furnace with a temperature-control heating device. The catalyst mass was 2 g for all experiments, and N_2 was used as the carrier gas in order to eliminate the entrapped oxygen gas from the reactor and was conducted under atmospheric pressure. The quartz reactor tube was heated by the temperature-control heating device, and the temperature of the catalyst bed was measured using calibrated thermocouples. After the catalyst's bed temperature was stable at 515 °C, WHSV (weight hourly space velocity) of the feedstock of 2.7 h⁻¹ was fed to the reactor by a constant flow pump. The reactor outlet product vapors were transformed to liquid by three groups of condensers, namely a 10 °C water condenser, a 0 °C ice-water bath, and a -190 °C liquid nitrogen trap. The major

products generated during the process were liquid, gaseous hydrocarbons, and coke. The collected liquid products consisting of aqueous and organic fractions were separated by centrifugation. The amount of the organic liquid product and the aqueous liquid product, namely OLP and ALP (H_2O was obtained from the reaction), were measured to give the yield of OLP and ALP, respectively. Additionally, the coke was determined from the difference in the weight of the reaction tube before and after the reaction. Finally, the gas products were collected by gas-collecting bags, and the yield was calculated by an overall mass balance. After 60 min of feeding, the feeding system was shut down, and nitrogen was used to purge for another 20 min before sampling. The reaction was repeated until the catalyst was deactivated.

4.5. Analytical Methods. The FT-IR (Thermo Fisher Nicolet Summit FTIR Spectrometer) analysis of the feedstocks and OLPs was performed in order to distinguish the characteristic peaks of functional groups, especially the oxygen-containing groups in the products. The wavenumber range was 4000–500 cm⁻¹.

The aromatic hydrocarbon content of the OLPs was measured by gas chromatography–mass spectrometry (Agilent 7890A/5975C) and gas chromatography (Agilent 7890A) equipped with a flame ionization detector (FID). Both GCs were equipped with a DB-35 capillary column (30 m × 0.32 mm × 0.25 μm). The methods were as follows: the temperature of the injector was set at 260 °C, the oven temperature was programmed to keep at 40 °C for 2 min and then increased to 90 °C at a rate of 10 °C/min and held at 90 °C for 2 min, after that heated to 180 °C at 5 °C/min for 2 min followed by heating at 10 °C/min to 280 °C, and held at 280 °C for 10 min. The EI voltage of the mass ion sources was 70 eV, and the mass spectral scanning range was 50–550 Da. An External standard was applied for the major aromatics such as benzene, toluene, *o*-xylene, *m*, *p*-xylene, naphthalene, 1-methylnaphthalene, 2-methylnaphthalene, and 2,6-dimethylnaphthalene.

The components of gaseous products (TOS of 60 min) were determined using a gas chromatography system (Agilent 7890B). The gas chromatographic system consisted of three detectors. An FID equipped with HP-AL/S and a DB-1 capillary column were used for the analysis of light hydrocarbons (C_1 – C_5). A thermal conductivity detector (TCD) with helium as the carrier gas was used for the analysis of CO , CO_2 , and N_2 , and another TCD with nitrogen as the carrier gas was used for the analysis of H_2 . The initial temperature of the oven was 60 °C and was maintained for 1 min and then increased to 80 °C at a rate of 20 °C/min, and after that, it was heated to 190 °C at a rate of 25 °C/min and maintained there for 1 min. The external standard method was applied for the quantification of gaseous products. Standard gas mixtures were used for calibration to obtain the peak retention time, peak area, and volume content. After the GC analysis of the gaseous product, the peak retention time and peak area of components were obtained. The relative content of components in the gaseous product was determined based on the relationship between the peak area and volume content.

■ ASSOCIATED CONTENT

SI Supporting Information

The Supporting Information is available free of charge at <https://pubs.acs.org/doi/10.1021/acsomega.2c02011>.

Catalyst characterization methods; simplified schematic diagram of reaction setups; FT-IR spectra of different feedstock oils and OLPs obtained by catalytic pyrolysis of glyceryl trioleate over different catalysts; compositions and total-ion chromatograms of OLPs obtained by catalytic pyrolysis of GT over different catalysts; total-ion chromatograms of OLPs obtained by catalytic pyrolysis of different feedstocks over Zn/HZSM-5 at a TOS of 60 min; catalyst reusability of Zn/HZSM-5 catalysts; and N₂ adsorption–desorption isothermals of deactivated catalysts (PDF)

AUTHOR INFORMATION

Corresponding Author

Fei Wang – Jiangsu Co-Innovation Center of Efficient Processing and Utilization of Forest Resources, College of Chemical Engineering, Nanjing Forestry University, Nanjing 210037, China; Jiangsu Provincial Key Lab for Chemistry and Utilization of Agro-Forest Biomass, Jiangsu Key Lab of Biomass-Based Green Fuels and Chemicals, Nanjing Forestry University, Nanjing 210037, China; orcid.org/0000-0001-6428-5111; Email: hgwf@njfu.edu.cn

Authors

Xiaoling Liu – Jiangsu Co-Innovation Center of Efficient Processing and Utilization of Forest Resources, College of Chemical Engineering, Nanjing Forestry University, Nanjing 210037, China; Jiangsu Provincial Key Lab for Chemistry and Utilization of Agro-Forest Biomass, Jiangsu Key Lab of Biomass-Based Green Fuels and Chemicals, Nanjing Forestry University, Nanjing 210037, China; orcid.org/0000-0003-0839-6356

Yafei Wu – Jiangsu Co-Innovation Center of Efficient Processing and Utilization of Forest Resources, College of Chemical Engineering, Nanjing Forestry University, Nanjing 210037, China; Jiangsu Provincial Key Lab for Chemistry and Utilization of Agro-Forest Biomass, Jiangsu Key Lab of Biomass-Based Green Fuels and Chemicals, Nanjing Forestry University, Nanjing 210037, China; orcid.org/0000-0003-4991-5036

Jun Zhang – Jiangsu Co-Innovation Center of Efficient Processing and Utilization of Forest Resources, College of Chemical Engineering, Nanjing Forestry University, Nanjing 210037, China; Jiangsu Provincial Key Lab for Chemistry and Utilization of Agro-Forest Biomass, Jiangsu Key Lab of Biomass-Based Green Fuels and Chemicals, Nanjing Forestry University, Nanjing 210037, China; orcid.org/0000-0002-6627-056X

Yu Zhang – Jiangsu Co-Innovation Center of Efficient Processing and Utilization of Forest Resources, College of Chemical Engineering, Nanjing Forestry University, Nanjing 210037, China; Jiangsu Provincial Key Lab for Chemistry and Utilization of Agro-Forest Biomass, Jiangsu Key Lab of Biomass-Based Green Fuels and Chemicals, Nanjing Forestry University, Nanjing 210037, China; orcid.org/0000-0002-2614-5975

Xun Li – Jiangsu Co-Innovation Center of Efficient Processing and Utilization of Forest Resources, College of Chemical Engineering, Nanjing Forestry University, Nanjing 210037, China; Jiangsu Provincial Key Lab for Chemistry and Utilization of Agro-Forest Biomass, Jiangsu Key Lab of Biomass-Based Green Fuels and Chemicals, Nanjing Forestry

University, Nanjing 210037, China; orcid.org/0000-0002-1267-9263

Haian Xia – Jiangsu Co-Innovation Center of Efficient Processing and Utilization of Forest Resources, College of Chemical Engineering, Nanjing Forestry University, Nanjing 210037, China; Jiangsu Provincial Key Lab for Chemistry and Utilization of Agro-Forest Biomass, Jiangsu Key Lab of Biomass-Based Green Fuels and Chemicals, Nanjing Forestry University, Nanjing 210037, China

Complete contact information is available at:

<https://pubs.acs.org/10.1021/acsomega.2c02011>

Notes

The authors declare no competing financial interest.

ACKNOWLEDGMENTS

The authors are highly grateful for the financial support from the National Key Research & Development Program of China (2019YFB1504002) and the Top-notch Academic Programs Project of Jiangsu Higher Education Institutions (PPZY2015C221).

REFERENCES

- (1) Yang, T.; Cheng, L.; Li, N.; Liu, D. Effect of Metal Active Sites on the Product Distribution over Composite Catalysts in the Direct Synthesis of Aromatics from Syngas. *Ind. Eng. Chem. Res.* **2017**, *56*, 11763–11772.
- (2) Yu, L.; Huang, S.; Zhang, S.; Liu, Z.; Xin, W.; Xie, S.; Xu, L. Transformation of Isobutyl Alcohol to Aromatics over Zeolite-Based Catalysts. *ACS Catal.* **2012**, *2*, 1203–1210.
- (3) Chen, X.; Dong, M.; Niu, X.; Wang, K.; Chen, G.; Fan, W.; Wang, J.; Qin, Z. Influence of Zn species in HZSM-5 on ethylene aromatization. *Chin. J. Catal.* **2015**, *36*, 880–888.
- (4) Tian, H.; Jiao, J.; Tian, H.; He, H.; Zha, F.; Guo, X.; Tang, X.; Chang, Y. Methanol aromatization over Zn-modified HZSM-5 catalysts derived from ZIF-8. *Fuel* **2021**, *302*, 121224.
- (5) Meindersma, G. W.; Podt, A.; Klaren, M. B.; de Haan, A. B. Separation of Aromatic and Aliphatic Hydrocarbons with Ionic Liquids. *Chem. Eng. Commun.* **2007**, *193*, 1384–1396.
- (6) Maher, K. D.; Bressler, D. C. Pyrolysis of triglyceride materials for the production of renewable fuels and chemicals. *Bioresour. Technol.* **2007**, *98*, 2351–2368.
- (7) Lok, C. M.; Van Doorn, J.; Aranda Almansa, G. Promoted ZSM-5 catalysts for the production of bio-aromatics, a review. *Renewable Sustainable Energy Rev.* **2019**, *113*, 109248.
- (8) Carlson, T. R.; Cheng, Y.-T.; Jae, J.; Huber, G. W. Production of green aromatics and olefins by catalytic fast pyrolysis of wood sawdust. *Energy Environ. Sci.* **2011**, *4*, 145–161.
- (9) Jing, Y.; Guo, Y.; Xia, Q.; Liu, X.; Wang, Y. Catalytic Production of Value-Added Chemicals and Liquid Fuels from Lignocellulosic Biomass. *Chem* **2019**, *5*, 2520–2546.
- (10) Carlson, T. R.; Tompsett, G. A.; Conner, W. C.; Huber, G. W. Aromatic Production from Catalytic Fast Pyrolysis of Biomass-Derived Feedstocks. *Top. Catal.* **2009**, *52*, 241–252.
- (11) He, S.; Muizebelt, I.; Heeres, A.; Schenk, N. J.; Bles, R.; Heeres, H. J. Catalytic pyrolysis of crude glycerol over shaped ZSM-5/bentonite catalysts for bio-BTX synthesis. *Appl. Catal., B* **2018**, *235*, 45–55.
- (12) Pattanaik, B. P.; Misra, R. D. Effect of reaction pathway and operating parameters on the deoxygenation of vegetable oils to produce diesel range hydrocarbon fuels: A review. *Renewable Sustainable Energy Rev.* **2017**, *73*, 545–557.
- (13) Atabani, A. E.; Silitonga, A. S.; Badruddin, I. A.; Mahlia, T. M. I.; Masjuki, H. H.; Mekhilef, S. A comprehensive review on biodiesel as an alternative energy resource and its characteristics. *Renewable Sustainable Energy Rev.* **2012**, *16*, 2070–2093.

- (14) Wang, L.; Lei, H.; Bu, Q.; Ren, S.; Wei, Y.; Zhu, L.; Zhang, X.; Liu, Y.; Yadavalli, G.; Lee, J.; Chen, S.; Tang, J. Aromatic hydrocarbons production from ex situ catalysis of pyrolysis vapor over Zinc modified ZSM-5 in a packed-bed catalysis coupled with microwave pyrolysis reactor. *Fuel* **2014**, *129*, 78–85.
- (15) Teixeira, C. M.; Fréty, R.; Barbosa, C. B. M.; Santos, M. R.; Bruce, E. D.; Pacheco, J. G. A. Mo influence on the kinetics of jatropha oil cracking over Mo/HZSM-5 catalysts. *Catal. Today* **2017**, *279*, 202–208.
- (16) Wang, J.; Zhong, Z.; Ding, K.; Zhang, B.; Deng, A.; Min, M.; Chen, P.; Ruan, R. Successive desilication and dealumination of HZSM-5 in catalytic conversion of waste cooking oil to produce aromatics. *Energy Convers. Manage.* **2017**, *147*, 100–107.
- (17) Heeres, A.; Schenk, N.; Muizebelt, I.; Bles, R.; De Waele, B.; Zeeuw, A.-J.; Meyer, N.; Carr, R.; Wilbers, E.; Heeres, H. J. Synthesis of Bio-aromatics from Black Liquors Using Catalytic Pyrolysis. *ACS Sustainable Chem. Eng.* **2018**, *6*, 3472–3480.
- (18) Twaiq, F. A.; Zabidi, N. A. M.; Mohamed, A. R.; Bhatia, S. Catalytic conversion of palm oil over mesoporous aluminosilicate MCM-41 for the production of liquid hydrocarbon fuels. *Fuel Process. Technol.* **2003**, *84*, 105–120.
- (19) Taufiqurrahmi, N.; Mohamed, A. R.; Bhatia, S. Production of biofuel from waste cooking palm oil using nanocrystalline zeolite as catalyst: process optimization studies. *Bioresour. Technol.* **2011**, *102*, 10686–10694.
- (20) Ooi, Y.-S.; Zakaria, R.; Mohamed, A. R.; Bhatia, S. Hydrothermal stability and catalytic activity of mesoporous aluminum-containing SBA-15. *Catal. Commun.* **2004**, *5*, 441–445.
- (21) Lovás, P.; Hudec, P.; Hadvinová, M.; Ház, A. Conversion of rapeseed oil via catalytic cracking: Effect of the ZSM-5 catalyst on the deoxygenation process. *Fuel Process. Technol.* **2015**, *134*, 223–230.
- (22) Liu, S.; Wu, G.; Syed-Hassan, S. S. A.; Li, B.; Hu, X.; Zhou, J.; Huang, Y.; Zhang, S.; Zhang, H. Catalytic pyrolysis of pine wood over char-supported Fe: Bio-oil upgrading and catalyst regeneration by CO₂/H₂O. *Fuel* **2022**, *307*, 121778.
- (23) Liu, S.; Wang, Y.; Wang, J.; Zhou, J.; Hu, X.; Sun, H.; Akhtar, M. A.; Zhang, H.; Huang, Y.; Zhang, S. Decomposition of benzyl phenyl ether over char-supported Ni: The effect of char structures. *Fuel Process. Technol.* **2021**, *221*, 106941.
- (24) Wang, F.; Chu, X.; Zhu, F.; Wu, F.; Li, Q.; Liu, B.; Xiao, G. Producing BTX aromatics-enriched oil from biomass derived glycerol using dealuminated HZSM-5 by successive steaming and acid leaching as catalyst: Reactivity, acidity and product distribution. *Microporous Mesoporous Mater.* **2019**, *277*, 286–294.
- (25) Hilten, R.; Speir, R.; Kastner, J.; Das, K. C. Production of aromatic green gasoline additives via catalytic pyrolysis of acidulated peanut oil soap stock. *Bioresour. Technol.* **2011**, *102*, 8288–8294.
- (26) Satyarthi, J. K.; Chiranjeevi, T.; Gokak, D. T.; Viswanathan, P. S. An overview of catalytic conversion of vegetable oils/fats into middle distillates. *Catal. Sci. Technol.* **2013**, *3*, 70–80.
- (27) Hartmann, M.; Machoke, A. G.; Schwieger, W. Catalytic test reactions for the evaluation of hierarchical zeolites. *Chem. Soc. Rev.* **2016**, *45*, 3313–3330.
- (28) Hartmann, M. Hierarchical zeolites: a proven strategy to combine shape selectivity with efficient mass transport. *Angew. Chem., Int. Ed.* **2004**, *43*, 5880–5882.
- (29) Botas, J. A.; Serrano, D. P.; García, A.; de Vicente, J.; Ramos, R. Catalytic conversion of rapeseed oil into raw chemicals and fuels over Ni- and Mo-modified nanocrystalline ZSM-5 zeolite. *Catal. Today* **2012**, *195*, 59–70.
- (30) Tan, S.; Zhang, Z.; Sun, J.; Wang, Q. Recent progress of catalytic pyrolysis of biomass by HZSM-5. *Chin. J. Catal.* **2013**, *34*, 641–650.
- (31) Li, Y.; Liu, S.; Xie, S.; Xu, L. Promoted metal utilization capacity of alkali-treated zeolite: Preparation of Zn/ZSM-5 and its application in 1-hexene aromatization. *Appl. Catal., A* **2009**, *360*, 8–16.
- (32) Li, Y.; Liu, S.; Zhang, Z.; Xie, S.; Zhu, X.; Xu, L. Aromatization and isomerization of 1-hexene over alkali-treated HZSM-5 zeolites: Improved reaction stability. *Appl. Catal., A* **2008**, *338*, 100–113.
- (33) Zheng, Y.; Wang, F.; Yang, X.; Huang, Y.; Liu, C.; Zheng, Z.; Gu, J. Study on aromatics production via the catalytic pyrolysis vapor upgrading of biomass using metal-loaded modified H-ZSM-5. *J. Anal. Appl. Pyrolysis* **2017**, *126*, 169–179.
- (34) Feng, F.; Wang, L.; Zhang, X.; Wang, Q. Self-Pillared ZSM-5-Supported Ni Nanoparticles as an Efficient Catalyst for Upgrading Oleic Acid to Aviation-Fuel-Range-Alkanes. *Ind. Eng. Chem. Res.* **2019**, *58*, 13112–13121.
- (35) Zhang, L.-Y.; Cao, J.-P.; Ren, X.-Y.; Feng, X.-B.; Wang, J.-X.; He, Z.-M.; Liu, T.-L.; Yang, Z.; Zhao, X.-Y.; Bai, H.-C. Catalytic Upgrading of Cellulose Pyrolysis Volatiles over Ce Modified Hierarchical ZSM-5 Zeolite: Insight into the Effect of Acid Properties on Light Aromatics and Catalyst Stability. *Ind. Eng. Chem. Res.* **2022**, *61*, 287–298.
- (36) Wang, J.-X.; Cao, J.-P.; Zhao, X.-Y.; Liu, S.-N.; Ren, X.-Y.; Zhang, L.-Y.; Feng, X.-B.; Zhao, Y.-P.; Wei, X.-Y. In Situ Upgrading of Cellulose Pyrolysis Volatiles Using Hydrofluorinated and Platinum-Loaded HZSM-5 for High Selectivity Production of Light Aromatics. *Ind. Eng. Chem. Res.* **2019**, *58*, 22193–22201.
- (37) Coqueblin, H.; Richard, A.; Uzio, D.; Pinard, L.; Pouilloux, Y.; Epron, F. Effect of the metal promoter on the performances of H-ZSM5 in ethylene aromatization. *Catal. Today* **2017**, *289*, 62–69.
- (38) Vichaphund, S.; Aht-ong, D.; Sricharoenchaikul, V.; Atong, D. Production of aromatic compounds from catalytic fast pyrolysis of Jatropha residues using metal/HZSM-5 prepared by ion-exchange and impregnation methods. *Renewable Energy* **2015**, *79*, 28–37.
- (39) Ishihara, A.; Kanamori, S.; Hashimoto, T. Effects of Zn Addition into ZSM-5 Zeolite on Dehydrocyclization-Cracking of Soybean Oil Using Hierarchical Zeolite-Al₂O₃ Composite-Supported Pt/NiMo Sulfided Catalysts. *ACS Omega* **2021**, *6*, 5509–5517.
- (40) Singh, O.; Agrawal, A.; Dhiman, N. Production of renewable aromatics from jatropha oil over multifunctional ZnCo/ZSM-5 catalysts. *Renewable Energy* **2021**, *179*, 2124–2135.
- (41) Li, M.; Xing, S.; Yang, L.; Fu, J.; Lv, P.; Wang, Z.; Yuan, Z. Nickel-loaded ZSM-5 catalysed hydrogenation of oleic acid: The game between acid sites and metal centres. *Appl. Catal., A* **2019**, *587*, 117112.
- (42) He, S.; Klein, F. G. H.; Kramer, T. S.; Chandel, A.; Tegudeer, Z.; Heeres, A.; Heeres, H. J. Catalytic Conversion of Free Fatty Acids to Bio-Based Aromatics: A Model Investigation Using Oleic Acid and an H-ZSM-5/Al₂O₃ Catalyst. *ACS Sustainable Chem. Eng.* **2021**, *9*, 1128–1141.
- (43) Bayat, A.; Sadrameli, S. M. Production of renewable aromatic hydrocarbons via conversion of canola oil methyl ester (CME) over zinc promoted HZSM-5 catalysts. *Renewable Energy* **2017**, *106*, 62–67.
- (44) Bayat, A. Enhanced Performance of Methyl Ester to Renewable Aromatics via Thermocatalytic Conversion over Metal-Modified HZSM-5 Zeolites: An Experimental Study. *ChemistrySelect* **2018**, *3*, 13338–13344.
- (45) Mo, N.; Savage, P. E. Hydrothermal Catalytic Cracking of Fatty Acids with HZSM-5. *ACS Sustainable Chem. Eng.* **2013**, *2*, 88–94.
- (46) Bielansky, P.; Weinert, A.; Schönberger, C.; Reichhold, A. Catalytic conversion of vegetable oils in a continuous FCC pilot plant. *Fuel Process. Technol.* **2011**, *92*, 2305–2311.
- (47) Mo, N.; Pennebacker, J.; Savage, P. E. Hydrocarbon chemicals from hydrothermal processing of renewable oils over HZSM-5. *Biomass Convers. Biorefin.* **2016**, *7*, 437–443.
- (48) Zheng, Z.; Wang, J.; Wei, Y.; Liu, X.; Yu, F.; Ji, J. Effect of La-Fe/Si-MCM-41 catalysts and CaO additive on catalytic cracking of soybean oil for biofuel with low aromatics. *J. Anal. Appl. Pyrolysis* **2019**, *143*, 104693.
- (49) Ramos, R.; García, A.; Botas, J. A.; Serrano, D. P. Enhanced Production of Aromatic Hydrocarbons by Rapeseed Oil Conversion over Ga and Zn Modified ZSM-5 Catalysts. *Ind. Eng. Chem. Res.* **2016**, *55*, 12723–12732.

- (50) Wang, F.; Zheng, Y.; Huang, Y.; Yang, X.; Xu, G.; Kang, J.; Liu, C.; Zheng, Z. Optimizing catalytic pyrolysis of rubber seed oil for light aromatics and anti-deactivation of ZSM-5. *J. Anal. Appl. Pyrolysis* **2017**, *126*, 180–187.
- (51) Zhang, J.; Wu, Z.; Li, X.; Zhang, Y.; Bao, Z.; Bai, L.; Wang, F. Catalytic Cracking of Inedible Oils for the Production of Drop-In Biofuels over a $\text{SO}_4^{2-}/\text{TiO}_2/\text{ZrO}_2$ Catalyst. *Energy Fuels* **2020**, *34*, 14204–14214.
- (52) Karnjanakom, S.; Yoshida, A.; Bayu, A.; Kurnia, I.; Hao, X.; Maneechakr, P.; Abudula, A.; Guan, G. Bifunctional Mg–Cu-Loaded β -Zeolite: High Selectivity for the Conversion of Furfural into Monoaromatic Compounds. *ChemCatChem* **2018**, *10*, 3564–3575.
- (53) Abdelsayed, V.; Smith, M. W.; Shekhawat, D. Investigation of the stability of Zn-based HZSM-5 catalysts for methane dehydroaromatization. *Appl. Catal., A* **2015**, *505*, 365–374.
- (54) Wei, Z.; Chen, L.; Cao, Q.; Wen, Z.; Zhou, Z.; Xu, Y.; Zhu, X. Steamed Zn/ZSM-5 catalysts for improved methanol aromatization with high stability. *Fuel Process. Technol.* **2017**, *162*, 66–77.
- (55) Oseke, G. G.; Atta, A. Y.; Mukhtar, B.; El-Yakubu, B. J.; Aderemi, B. O. Increasing the catalytic stability of microporous Zn/ZSM-5 with copper for enhanced propane aromatization. *J. King Saud Univ., Eng. Sci.* **2020**, *33*, 531–538.
- (56) Che, Q.; Yang, M.; Wang, X.; Yang, Q.; Rose Williams, L.; Yang, H.; Zou, J.; Zeng, K.; Zhu, Y.; Chen, Y.; Chen, H. Influence of physicochemical properties of metal modified ZSM-5 catalyst on benzene, toluene and xylene production from biomass catalytic pyrolysis. *Bioresour. Technol.* **2019**, *278*, 248–254.
- (57) Jia, Y.; Wang, J.; Zhang, K.; Feng, W.; Liu, S.; Ding, C.; Liu, P. Promoted effect of zinc–nickel bimetallic oxides supported on HZSM-5 catalysts in aromatization of methanol. *J. Energy Chem.* **2017**, *26*, 540–548.
- (58) Song, C.; Li, X.; Zhu, X.; Liu, S.; Chen, F.; Liu, F.; Xu, L. Influence of the state of Zn species over Zn-ZSM-5/ZSM-11 on the coupling effects of cofeeding n-butane with methanol. *Appl. Catal., A* **2016**, *519*, 48–55.
- (59) Liu, J.; He, N.; Zhou, W.; Lin, L.; Liu, G.; Liu, C.; Wang, J.; Xin, Q.; Xiong, G.; Guo, H. Isobutane aromatization over a complete Lewis acid Zn/HZSM-5 zeolite catalyst: performance and mechanism. *Catal. Sci. Technol.* **2018**, *8*, 4018–4029.
- (60) Gabrienko, A. A.; Arzumanov, S. S.; Toktarev, A. V.; Danilova, I. G.; Prosvirin, I. P.; Kriventsov, V. V.; Zaikovskii, V. I.; Freude, D.; Stepanov, A. G. Different Efficiency of Zn^{2+} and ZnO Species for Methane Activation on Zn-Modified Zeolite. *ACS Catal.* **2017**, *7*, 1818–1830.
- (61) Liu, D.; Cao, L.; Zhang, G.; Zhao, L.; Gao, J.; Xu, C. Catalytic conversion of light alkanes to aromatics by metal-containing HZSM-5 zeolite catalysts—A review. *Fuel Process. Technol.* **2021**, *216*, 106770.
- (62) Fadaeeraeyeni, S.; Shan, J.; Sarnello, E.; Xu, H.; Wang, H.; Cheng, J.; Li, T.; Toghiani, H.; Xiang, Y. Nickel/gallium modified HZSM-5 for ethane aromatization: Influence of metal function on reactivity and stability. *Appl. Catal., A* **2020**, *601*, 117629.
- (63) Tian, H.; Liao, J.; Zha, F.; Guo, X.; Tang, X.; Chang, Y.; Ma, X. Catalytic Performance of In/HZSM-5 for Coupling Propane with CO_2 to Propylene. *ChemistrySelect* **2020**, *5*, 3626–3637.
- (64) Shi, Y.; Gao, C.; Xing, E.; Zhang, J.; Duan, F.; Zhao, H.; Xie, Y. Ni nanoparticles encapsulated within H-type ZSM-5 crystals for upgrading palmitic acid to diesel-like fuels. *Chin. Chem. Lett.* **2022**, *33*, 803–806.
- (65) Zhang, J.; Shi, Y.; Cao, H.; Wu, Y.; Yang, M. Conversion of palmitic acid to jet fuel components over Mo/H-ZSM-22 bifunctional catalysts with high carbon reservation. *Appl. Catal., A* **2020**, *608*, 117847.
- (66) Tamiyakul, S.; Anutamjarikun, S.; Jongpatiwut, S. The effect of Ga and Zn over HZSM-5 on the transformation of palm fatty acid distillate (PFAD) to aromatics. *Catal. Commun.* **2016**, *74*, 49–54.
- (67) Serykh, A. I. On photoluminescence properties of gallium-exchanged ZSM-5 zeolite. *Chem. Phys. Lett.* **2012**, *554*, 159–162.
- (68) Serykh, A. I. Optical properties of indium-exchanged mordenite zeolite. *Microporous Mesoporous Mater.* **2019**, *275*, 147–151.
- (69) Phung, T. K.; Radikapratama, R.; Garbarino, G.; Lagazzo, A.; Riani, P.; Busca, G. Tuning of product selectivity in the conversion of ethanol to hydrocarbons over H-ZSM-5 based zeolite catalysts. *Fuel Process. Technol.* **2015**, *137*, 290–297.
- (70) Mhamdi, M.; Ghorbel, A.; Delahay, G. Influence of the V+Mo/Al ratio on vanadium and molybdenum speciation and catalytic properties of V–Mo–ZSM-5 prepared by solid-state reaction. *Catal. Today* **2009**, *142*, 239–244.
- (71) Wei, C.-L.; Gao, J.; Wang, K.; Dong, M.; Fan, W.-B.; Qin, Z.-F.; Wang, J.-G. Effect of Hydrogen pre-treatment on the catalytic properties of Zn/HZSM-5 zeolite for ethylene aromatization reaction. *Acta Phys.-Chim. Sin.* **2017**, *33*, 1483–1491.
- (72) Avasavasukhi, A.; Sooknoi, T. Tunable activity of [Ga]HZSM-5 with H_2 treatment: Ethane dehydrogenation. *Catal. Commun.* **2014**, *45*, 63–68.
- (73) Zhao, X.; Wei, L.; Julson, J.; Gu, Z.; Cao, Y. Catalytic cracking of inedible camelina oils to hydrocarbon fuels over bifunctional Zn/ZSM-5 catalysts. *Korean J. Chem. Eng.* **2015**, *32*, 1528–1541.
- (74) Cerqueira, H. S.; Caeiro, G.; Costa, L.; Ramôa Ribeiro, F. Deactivation of FCC catalysts. *J. Mol. Catal. A: Chem.* **2008**, *292*, 1–13.
- (75) Fan, Y.; Cai, Y.; Li, X.; Yin, H.; Xia, J. Coking characteristics and deactivation mechanism of the HZSM-5 zeolite employed in the upgrading of biomass-derived vapors. *J. Ind. Eng. Chem.* **2017**, *46*, 139–149.
- (76) Wang, H.-Z.; Sun, L.-L.; Sui, Z.-J.; Zhu, Y.-A.; Ye, G.-H.; Chen, D.; Zhou, X.-G.; Yuan, W.-K. Coke Formation on Pt–Sn/ Al_2O_3 Catalyst for Propane Dehydrogenation. *Ind. Eng. Chem. Res.* **2018**, *57*, 8647–8654.
- (77) Kubátová, A.; Geetla, A.; Casey, J.; Linnen, M. J.; Seames, W. S.; Smoliakova, I. P.; Kozliak, E. I. Cleavage of Carboxylic Acid Moieties in Triacylglycerides During Non-Catalytic Pyrolysis. *J. Am. Oil Chem. Soc.* **2015**, *92*, 755–767.
- (78) Sembiring, K. C.; Aunillah, A.; Minami, E.; Saka, S. Renewable gasoline production from oleic acid by oxidative cleavage followed by decarboxylation. *Renewable Energy* **2018**, *122*, 602–607.